

Helicity conservation in nonlinear mean-field solar dynamo

V.V. Pipin^{1,2}, D.D. Sokoloff^{1,3}, H.Zhang¹, K.M. Kuzanyan^{1,4,1}

^{1 1} Key Laboratory of Solar Activity, National Astronomical Observatories,
Chinese Academy of Sciences, Beijing 100012, China

² Institute of Solar-Terrestrial Physics, Russian Academy of Sciences, Irkutsk, 664033, Russia

³ Department of Physics, Moscow University, 119992 Moscow, Russia

⁴ IZMIRAN, Russian Academy of Sciences, Troitsk, Moscow region 142190, Russia

We explore the impact of magnetic helicity conservation on the mean-field solar dynamo using the axisymmetric dynamo model which includes the subsurface shear. Our results support the recent findings by Hubbard & Brandenburg [6], who suggested that the catastrophic quenching in the mean-field dynamo is alleviated if conservation of the total magnetic helicity is taken into account. We show that the solar dynamo can operate in the wide range of the magnetic Reynolds number up to 10^6 . We also found that the boundary conditions for the magnetic helicity influence the distribution of the α -effect near the solar surface.

Keywords: Turbulence: Mean-field magnetohydrodynamics; Sun: magnetic field; Stars: activity – Dynamo

PACS numbers:

INTRODUCTION

The basic idea for the solar dynamo action was developed by Parker [13]. He suggested that the toroidal component of the magnetic field of the Sun is stretched from the poloidal component by the differential rotation (Ω effect) and the cyclonic motions (α effect) return the part of the toroidal magnetic field energy back to the poloidal component. This is the so-called $\alpha\Omega$ scenario. This mechanism is implemented in the wide range of the solar dynamo models (see review by 4).

The effect of the turbulence in the mean-field dynamo is represented by the mean electromotive force $\mathcal{E} = \overline{\mathbf{u} \times \mathbf{b}}$, where \mathbf{u} and \mathbf{b} are the fluctuating velocity and magnetic fields. In the simplest case it can be found that $\mathcal{E} = \alpha_0 \overline{\mathbf{B}} + (\overline{\mathbf{V}^{(p)}} \times \overline{\mathbf{B}}) - \eta_T (\nabla \times \overline{\mathbf{B}})$, where α_0 is the α effect, $\overline{\mathbf{V}^{(p)}}$ is the turbulent pumping and η_T is the turbulent diffusivity [10]. The α effect is a pseudo-scalar (lacks the mirror symmetry) which is related to the kinetic helicity of the small-scale flows, i.e., $\alpha_0 = -\frac{\tau_c}{3} \overline{\mathbf{u} \cdot \nabla \times \mathbf{u}}$, where τ_c is correlation time of turbulent motion. Pouquet et al. [19] showed that the α effect is produced not only by kinetic helicity but also by current helicity, and it is $\alpha_0 = -\frac{\tau_c}{3} \left(\overline{\mathbf{u} \cdot \nabla \times \mathbf{u}} - \frac{\overline{\mathbf{b} \cdot \nabla \times \mathbf{b}}}{2\mu\bar{\rho}} \right)$. The latter effect can be interpreted as resistance of magnetic fields against the twist by helical motions. It leads to the concept of the catastrophic quenching of the α effect by the generated large-scale magnetic field. It was found that $\alpha_0(\overline{B}) = \frac{\alpha_0(0)}{1 + R_m(\overline{B}/\overline{B}_{eq})^2}$, where R_m is magnetic Reynolds number (see, 9 and references therein). In case of $R_m \gg 1$, the α effect is quickly saturated for the large-scale magnetic field strength that is much below the

equipartition value $\overline{B}_{eq} \sim \sqrt{\bar{\rho}\mu_0\bar{u}^2}$. The result was confirmed by the direct numerical simulations (DNS) [12]. The catastrophic quenching (CQ) is related to the dynamical quenching of the α effect. It is based on conservation of the magnetic helicity, $\overline{\chi} = \overline{\mathbf{a} \cdot \mathbf{b}}$ (\mathbf{a} is fluctuating part of the vector potential) and the relation between the current and magnetic helicities $h_C = \overline{\mathbf{b} \cdot \nabla \times \mathbf{b}} \sim \overline{\chi}/\ell^2$, which is valid for the isotropic turbulence [11]. The evolution equation for $\overline{\chi}$ can be obtained from equations that govern \mathbf{a} and \mathbf{b} , it reads as follows [9]:

$$\frac{\partial \overline{\chi}}{\partial t} = -2(\mathcal{E} \cdot \overline{\mathbf{B}}) - \frac{\overline{\chi}}{R_m \tau_c} - \nabla \cdot \mathcal{F}^\chi - \eta \overline{\mathbf{B}} \cdot \overline{\mathbf{J}}, \quad (1)$$

where, in following to Kleeeorin & Rogachevskii [9], we introduce the helicity fluxes $\mathcal{F}^\chi = \overline{\mathbf{a} \times \mathbf{u} \times \mathbf{B}} - \mathbf{a} \times (\mathbf{u} \times \mathbf{b})$. The helicity fluxes are capable to alleviate the catastrophic quenching (see, e.g., 3, 24 and references therein). Generally, it was found that the diffusive fluxes, which are $\sim \eta_\chi \nabla \overline{\chi}$, where η_χ is the turbulent diffusivity of the magnetic helicity, work robustly in the mean-field dynamo models but it requires $\eta_\chi > \eta_T$ to reach $|\overline{B}| \geq 0.1 \overline{B}_{eq}$.

Another possibility to alleviate the catastrophic quenching is related with the non-local formulation of the mean-electromotive force [2]. In fact, the Babcock-Leighton (BL) type dynamo is the special case of the mean-field dynamo with the nonlocal α effect. Kitchatinov & Olemskoy [8] found that the nonlocal α effect and the diamagnetic pumping can alleviate the catastrophic quenching. The results by Brandenburg & Käpylä [1] show that the strength of the quenching can depend on the model design. Therefore, the problem of the catastrophic quenching is actual for different types of the solar dynamo.

Recently, Hubbard & Brandenburg [6] revisited the concept of catastrophic quenching and showed that for

the shearing dynamos the Eq.(1) produces the nonphysical fluxes of the magnetic helicity over the spatial scales. They suggested to cure the problem using the global conservation law for the total magnetic helicity that can be written as follows:

$$\frac{d}{dt} \int \{\bar{\chi} + \bar{\mathbf{A}} \cdot \bar{\mathbf{B}}\} dV = -\eta \int \{\bar{\mathbf{B}} \cdot \bar{\mathbf{J}} + \bar{\mathbf{b}} \cdot \mathbf{j}\} dV \quad (2)$$

$$- \int \nabla \cdot \mathcal{F}^\chi dV$$

where integration is done over the volume that comprises the ensemble of the small-scale fields. We assume that \mathcal{F}^χ is the diffusive flux of the total helicity which is resulted from the turbulent motions. Ignoring the effect of the meridional circulation we write the local version of the Eq.(2) as follows [6]:

$$\frac{\partial \bar{\chi}}{\partial t} = -\frac{\partial (\bar{\mathbf{A}} \cdot \bar{\mathbf{B}})}{\partial t} - \frac{\bar{\chi}}{R_m \tau_c} - \eta \bar{\mathbf{B}} \cdot \bar{\mathbf{J}} - \nabla \cdot \mathcal{F}^\chi, \quad (3)$$

where $\mathcal{F}^\chi = -\eta_\chi \nabla (\bar{\chi} + \bar{\mathbf{A}} \cdot \bar{\mathbf{B}})$. In the paper we employ this equation for the dynamical quenching of the α effect in the solar dynamo model and show how it works in the range of the magnetic Reynolds number $R_m = 10^{3-6}$ those are typical for the astrophysical conditions.

BASIC EQUATIONS

We study the mean-field induction equation in a perfectly conducting medium:

$$\frac{\partial \bar{\mathbf{B}}}{\partial t} = \nabla \times (\mathcal{E} + \bar{\mathbf{U}} \times \bar{\mathbf{B}}), \quad (4)$$

where $\mathcal{E} = \overline{\mathbf{u} \times \mathbf{b}}$ is the mean electromotive force, with \mathbf{u}, \mathbf{b} being fluctuating velocity and magnetic field, respectively, $\bar{\mathbf{U}}$ is the mean velocity (differential rotation), and the axisymmetric magnetic field is:

$$\bar{\mathbf{B}} = e_\phi B + \nabla \times \frac{A e_\phi}{r \sin \theta},$$

where θ is the polar angle. The mean electromotive force \mathcal{E} is given by Pipin [14]. It is expressed as follows:

$$\mathcal{E}_i = \left(\alpha_{ij} + \gamma_{ij}^{(\Lambda)} \right) \bar{B}_j - \eta_{ijk} \nabla_j \bar{B}_k. \quad (5)$$

The tensor α_{ij} represents the α -effect, $\gamma_{ij}^{(\Lambda)}$ is the turbulent pumping, and η_{ijk} is the diffusivity tensor. The α effect includes hydrodynamic and magnetic helicity contributions,

$$\alpha_{ij} = C_\alpha \sin^2 \theta \alpha_{ij}^{(H)} + \alpha_{ij}^{(M)} \quad (6)$$

The details in expressions for the kinetic part of the α effect $\alpha_{ij}^{(H)}$, as well as $\gamma_{ij}^{(\Lambda)}$ and η_{ijk} can be found in [18].

The contribution of small-scale magnetic helicity $\bar{\chi} = \overline{\mathbf{a} \cdot \mathbf{b}}$ (\mathbf{a} is the fluctuating vector-potential of the magnetic field) to the α -effect is defined as

$$\alpha_{ij}^{(M)} = 2f_2^{(a)} \delta_{ij} \frac{\bar{\chi} \tau_c}{\mu_0 \rho \ell^2} - 2f_1^{(a)} e_i e_j \frac{\bar{\chi} \tau_c}{\mu_0 \rho \ell^2}. \quad (7)$$

The nonlinear feedback of the large-scale magnetic field to the α -effect is described by a dynamical quenching due to the constraint of magnetic helicity conservation given by Eq.(3). The effect of turbulent diffusivity, which is anisotropic due to the Coriolis force, is given by:

$$\eta_{ijk} = 3\eta_T \left\{ \left(2f_1^{(a)} - f_2^{(d)} \right) \varepsilon_{ijk} - 2f_1^{(a)} e_i e_n \varepsilon_{njk} \right. \quad (8)$$

$$\left. + C_\delta f_4^{(d)} e_j \delta_{ik} \right\},$$

where functions $f_{\{1,2,4\}}^{(a,d)}$ depend on the Coriolis number. They can be found in Pipin [14]. The last part of Eq. (8) stands for the $\Omega \times J$ effect [20]. The DNS dynamo experiments support the existence of the dynamo effects induced by the large-scale current and global rotation [7, 21].

We matched the potential field outside and the perfect conductivity at the bottom boundary with the standard boundary conditions. For the magnetic helicity we employ $\bar{\chi} = 0$ at the bottom of the convection zone. At the top we use two types of the boundary conditions like

$$\nabla_r \bar{\chi} = 0, \quad (9)$$

$$\nabla_r (\bar{\chi} + \bar{\mathbf{A}} \cdot \bar{\mathbf{B}}) = 0. \quad (10)$$

To evolve the Eq.(3) we have to define the large-scale vector potential for each time-step. For the axisymmetric large-scale magnetic fields where the vector-potential is $\bar{\mathbf{A}} = e_\phi A / (r \sin \theta) + r e_r T$. The toroidal part of the vector potential is governed by the dynamo equations. The poloidal part of the vector potential can be restored from equation $\nabla \times (r\mathbf{T}) = e_\phi B$. The restoration procedure is trivial for the pseudo-spectral numerical schemes which are based on the Legendre polynomial decomposition for the latitude profile of the large-scale toroidal field. The choice of parameters in the dynamo is justified by our previous studies [15]. Here we use $C_\alpha = 0.03$, $C_\delta = \frac{1}{3} C_\alpha$ and the diffusivity dilution factor $C_\eta = 0.1$. The parameters of the models are summarized in the Table I.

We estimate the turbulent parameters in the model on the base of the mixing-length theory and use as the reference the solar interior model computed by Stix [23]. The differential rotation profile is like that suggested by Pipin & Kosovichev [17]. Fig. 1 shows the radial profiles of the α effect components and profiles of the background turbulent diffusivity $C_\eta \eta_T$, the isotropic, $\eta^{(I)}$, and anisotropic, $\eta^{(A)}$, parts of the magnetic diffusivity as well as profile for the $\Omega \times J$ effect. To quantify the mirror

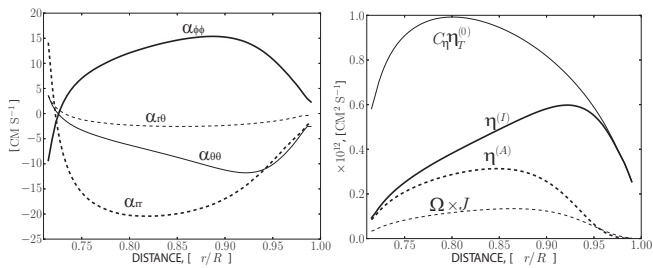


Figure 1: Left, (a), the profiles of the α effects components for the $\theta = 45^\circ$. Right, (b), the profiles of the background turbulent diffusivity $C_\eta \eta_T$, the isotropic, $\eta^{(I)}$, and anisotropic, $\eta^{(A)}$, parts of the magnetic diffusivity and $\Omega \times J$ effect (also known as δ effect [20]).

Table I: Summary of parameters of the models. Here, QT stands for the quenching type and BC - the boundary conditions.

Model	QT1 ₁ , QT2 ₁	QT1 _{2,3}	QT2 _{2,3}
R_χ	10^6	$10^3, 10^5$	$10^3, 10^5$
QT	Eq. (13), Eq. (3)	Eq. (3)	Eq. (1)
η_χ	$10^{-5} \eta_T$	$10^{-2} \eta_T$	$10^{-2} \eta_T$
BC	Eq. (9)	Eq. (9)	Eq. (9), Eq. (10)

symmetry type of the toroidal magnetic field distribution relative to equator we introduce the parity index P :

$$P = \frac{E_q - E_d}{E_q + E_d},$$

$$E_d = \int (B(r_0, \theta) - B(r_0, \pi - \theta))^2 \sin \theta d\theta,$$

$$E_q = \int (B(r_0, \theta) + B(r_0, \pi - \theta))^2 \sin \theta d\theta,$$

where E_d and E_q are the energies of the dipole-like and quadrupole-like modes, $r_0 = 0.9R_\odot$. We define the dynamical quenching type 1 (QT1) to be governed by Eq.(1), and the dynamical quenching type 2 (QT2) - by Eq. (3).

RESULTS

Fig. 2 shows the long-term evolution of the maximum of the large-scale magnetic field strength in the convection zone and the parity in the models. The energy of the toroidal magnetic fields in all models show the exponential growth in the beginning phase, which has duration about 10 diffusive time of the system. The greater initial magnetic field strength, the shorter duration of the exponential growth phase. Two models QT1₁ and QT2₁ have rather small diffusive fluxes of the helicity and the high magnetic Reynolds number $R_m = 10^6$. We consider them as the references. It is shown below, see Figures 2 and 4 that the model QT2₁ is not subjected to the catastrophic quenching while the model QT1₁ saturates the toroidal magnetic field strength to the level that is

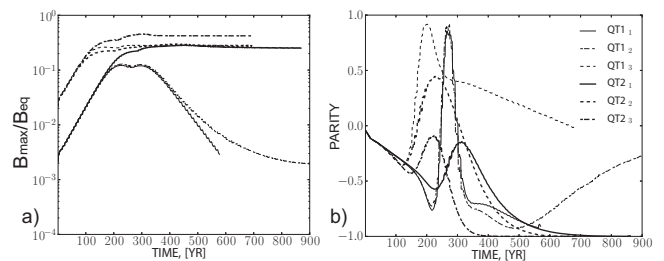


Figure 2: Left panel (a) shows the ratio of the maxima of the toroidal magnetic field strength and the equipartition value with time; (b) shows the parity indexes evolution in the models. We employ the running average to filter out the separate cycles.

much below the equipartition. The moderate diffusive flux with $\eta_\chi = 0.01\eta_T$ (model QT1₃) does not alleviate the problem if the magnetic helicity evolution is governed by the Eq. (1). In the models QT1₂ and QT2_{1,3} the saturation level of the toroidal magnetic field strength is about $0.3B_{eq}$, where B_{eq} is the equipartition level of the magnetic field strength. It is about $0.5B_{eq}$ in the model QT2₂ which has $R_m = 10^3$. The saturation level in the QT2 types solar dynamo can be higher for the greater C_α . This question needs a separate study. In the model QT1₁ as well as in all the QT2 models the parity index saturates to the dipole-like solution. In the QT1_{2,3} models the asymptotic stage is not clear and they need much longer runs.

The origin of difference in behaviour of the magnetic helicity evolution in the models with QT1 and QT2 has been discussed recently by Hubbard & Brandenburg [6]. Taking into the dynamo equation (4), the corresponding equation for the large-scale vector potential:

$$\frac{\partial \bar{\mathbf{A}}}{\partial t} = \boldsymbol{\mathcal{E}} + \bar{\mathbf{U}} \times \bar{\mathbf{B}}, \quad (11)$$

where we assume the Coulomb gauge, we find the equation which governs the large-scale helicity evolution:

$$\frac{\partial (\bar{\mathbf{A}} \cdot \bar{\mathbf{B}})}{\partial t} = 2\boldsymbol{\mathcal{E}} \cdot \bar{\mathbf{B}} + \nabla \cdot ((\boldsymbol{\mathcal{E}} \times \bar{\mathbf{A}}) - \bar{\mathbf{A}} \times (\bar{\mathbf{U}} \times \bar{\mathbf{B}})) \quad (12)$$

Therefore, Eq. (3) can be rewritten in form of Eq.(2):

$$\frac{\partial \bar{\chi}}{\partial t} = -2(\boldsymbol{\mathcal{E}} \cdot \bar{\mathbf{B}}) - \frac{\bar{\chi}}{R_m \tau_c} + \nabla \cdot (\eta_\chi \nabla \bar{\chi}) - \eta \bar{\mathbf{B}} \cdot \bar{\mathbf{J}} - \nabla \cdot (\boldsymbol{\mathcal{E}} \times \bar{\mathbf{A}}).$$

The term $(\boldsymbol{\mathcal{E}} \times \bar{\mathbf{A}})$ consists of the counterparts of the sources magnetic helicity, which are represented by $-2\boldsymbol{\mathcal{E}} \cdot \bar{\mathbf{B}}$, and the fluxes which result from pumping of the large-scale magnetic fields. The sources magnetic helicity in the term $-2(\boldsymbol{\mathcal{E}} \cdot \bar{\mathbf{B}})$ are partly compensated in Eq(13) by the counterparts in $(\boldsymbol{\mathcal{E}} \times \bar{\mathbf{A}})$. This results in the spatially homogeneous quenching of the large-scale magnetic

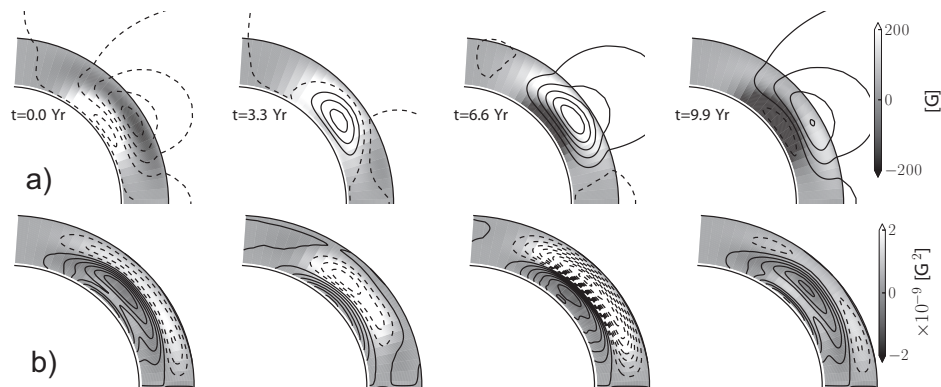


Figure 3: Snapshots of the magnetic field and helicity evolution inside the North segment of the convection zone for the model QT₂₃. Panel (a) shows the field lines of the poloidal component of the mean magnetic field and the toroidal magnetic field (varies ± 700 G) by gray scale density plot. The bottom panel, (b), shows the large-scale (density plot) and small-scale magnetic helicity (contours) distributions. Both kinds of the magnetic helicity vary in the same range of magnitude.

generation and alleviation of the catastrophic quenching problem. The last term in Eq(12) contains the transport of the large-scale magnetic helicity by the large-scale flow.

Fig. 3 shows the snapshots of the magnetic field and magnetic helicity (large- and small-scale) evolution in the North segment of the solar convection zone for the model QT₂₃. We observe the drift of the dynamo waves which are related to the large-scale toroidal and poloidal fields towards the equator and towards the pole, respectively. The distributions of the large- and small-scale magnetic helicities show the correspondence in sign: positive to negative, and the other way around, respectively. This is in agreement with Eq. (3). It is seen that the negative sign of the magnetic helicity follows the dynamo wave of the toroidal magnetic field. This can be related to the so-called “current helicity hemispheric sign rule” (negative/positive sign of helicity dominate in the North/South hemisphere) which is suggested by the observations (see Seehafer [22], Zhang et al. [26] and references therein). The origin of the helicity sign rule has been extensively studied in the dynamo theory (e.g., 5, 25). The similar snapshots for the QT1 model can be found in [16]. The main difference is that for the QT1 model all the changes in the magnetic helicity evolution does not exactly follow to the dynamo wave inside the convection zone as it is demonstrated for the QT2 model.

Fig. 4 shows variations of the radial profiles of the α effect and magnetic helicity with the cycle and the time-latitude diagrams for the dynamo model QT₂₃. For all the models the changes in the α effect are concentrated to the top of the convection zone. This is due to the factor $(\bar{\rho}\ell^2)^{-1}$ in relation between the current and magnetic helicities. The difference in the boundary at the top results in different distributions of the α effect in the models QT₂₁ and QT₂₃. We would like to notice that the QT₁₂ and QT₂₁ have the same boundary conditions, however, the resulted distributions of the α effect differ

drastically. The time-latitude diagrams for the dynamo model QT₂₃ which are shown in Figure 4, are in qualitative agreement with observations. The same patterns are obtained in the models QT_{21,2}. We show the dynamical α effect as well. The model shows that with the boundary conditions given by Eq. (10) the α effect increases and has positive maxima at the growing phase of the cycle and it decreases, having the negative minima at the decaying phase of the cycle.

CONCLUSION

In the paper we studied the effect of the magnetic helicity conservation in the mean-field solar dynamo model which is shaped by the subsurface shear. The results show that the solar dynamo can operate in the wide range of the magnetic Reynolds number up to 10^6 if conservation of the total magnetic helicity is taken into account.

It was found that the boundary conditions for the magnetic helicity influence the distribution of the α effect near the solar surface. For example, the dynamo wave becomes closer to equator when the diffusive flux of the total helicity is zero at the top of the convection zone because the dynamical increase of the α effect follows the dynamo wave (see Fig. 3, 4). The situation is opposite for the case when the diffusive flux is dominated by the large-scale helicity. Thus, the parity breaking in the solar dynamo can occur due to perturbations in the external boundary for the magnetic helicity. However, these points remain an open field for the future work.

V.P., D.S. and K.K. would like to acknowledge support from Visiting Professorship Programme of Chinese Academy of Sciences 2009J2-12 and thank NAOC of CAS for hospitality, as well as acknowledge the support of the Integration Project of SB RAS N 34, and support of the state contracts 02.740.11.0576, 16.518.11.7065 of the Ministry of Education and Science of Russian Fed-

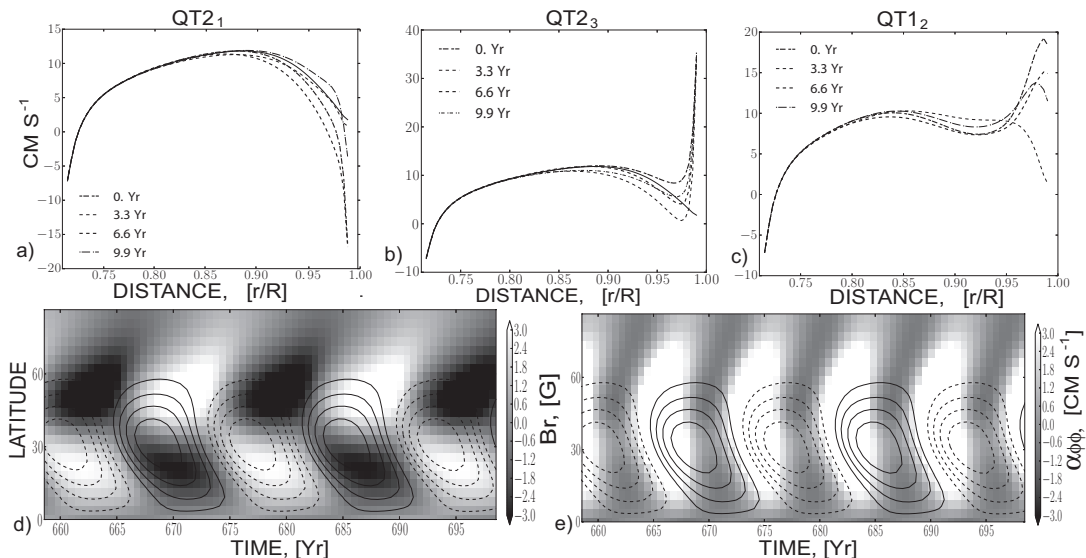


Figure 4: First row, (a,b and c), shows variations of the α effect ($\alpha_{\phi\phi}$ component) profiles with the cycle at colatitude $\theta = 45^\circ$, for the model QT2₁, QT2₃ and QT1₂ (from left to right). The bottom, panel (d) shows the time - latitude variations of the toroidal field near the surface, $r = 0.95R_\odot$, (contours $\pm 300\text{G}$) and the radial magnetic field at the surface (density plot) for the model QT2₃; panel (e) shows the same for the the toroidal field and the α effect ($\alpha_{\phi\phi}$ component)(density plot).

eration. H.Z. would like to acknowledge support from National Natural Science Foundation of China grants: 41174153 and 10921303.

-
- [1] Brandenburg, A., & Käpylä, P. J. 2007, *New Journal of Physics*, 9, 305
- [2] Brandenburg, A., Rädler, K.-H., & Schrunner, M. 2008, *A & A*, 482, 739
- [3] Brandenburg, A., & Subramanian, K. 2005, *Phys. Rep.*, 417, 1
- [4] Charbonneau, P. 2005, *Living Reviews in Solar Physics*, 2, 2
- [5] Choudhuri, A. R., Chatterjee, P., & Nandy, D. 2004, *ApJL*, 615, L57
- [6] Hubbard, A., & Brandenburg, A. 2012, *Astrophys. J.*, 748, 51
- [7] Käpylä, P. J., Korpi, M. J., & Brandenburg, A. 2008, *A & A*, 491, 353
- [8] Kitchatinov, L. L., & Olemskoy, S. V. 2011, *Astronomy Letters*, 37, 286
- [9] Kleeorin, N., & Rogachevskii, I. 1999, *Phys. Rev.E*, 59, 6724
- [10] Krause, F., & Rädler, K.-H. 1980, *Mean-Field Magnetohydrodynamics and Dynamo Theory* (Berlin: Akademie-Verlag), 271
- [11] Moffatt, H. K. 1978, *Magnetic Field Generation in Electrically Conducting Fluids* (Cambridge, England: Cambridge University Press)
- [12] Ossendrijver, M., Stix, M., & Brandenburg, A. 2001, *A & A*, 376, 713
- [13] Parker, E. 1955, *Astrophys. J.*, 122, 293
- [14] Pipin, V. V. 2008, *Geophysical and Astrophysical Fluid Dynamics*, 102, 21
- [15] Pipin, V. V., & Kosovichev, A. G. 2011, *Astrophys. J.*, 738, 104
- [16] —. 2011, *ApJ*, 741, 1
- [17] —. 2011, *ApJL*, 727, L45
- [18] Pipin, V. V., Sokoloff, D. D., & Usoskin, I. G. 2012, *A & A*, 542, A26
- [19] Pouquet, A., Frisch, U., & Léorat, J. 1975, *J. Fluid Mech.*, 68, 769
- [20] Rädler, K.-H. 1969, *Monats. Dt. Akad. Wiss.*, 11, 194
- [21] Schrunner, M. 2011, *A & A*, 533, A108
- [22] Seehafer, N. 1990, *Sol.Phys.*, 125, 219
- [23] Stix, M. 2002, *The sun: an introduction*, 2nd edn. (Berlin : Springer), 521
- [24] Vishniac, E. T., & Cho, J. 2001, *Astrophys. J.*, 550, 752
- [25] Zhang, H., Moss, D., Kleeorin, N., Kuzanyan, K., Rogachevskii, I., Sokoloff, D., Gao, Y., & Xu, H. 2012, *Astrophys. J.*, 751, 47
- [26] Zhang, H., Sakurai, T., Pevtsov, A., Gao, Y., Xu, H., Sokoloff, D. D., & Kuzanyan, K. 2010, *MNRAS*, 402, L30